Polarization-correlation mapping of biological tissue coherent images

O. V. Angelsky
A. G. Ushenko
Yu. A. Ushenko
Ye. G. Ushenko
Yu. Ya. Tomka
Chernivtsi National University
2 Kotsyubinsky Street
Chernivtsi 58012, Ukraine
E-mail: ushenko-bio@itf.cv.ukrtel.net

V. P. Pishak
Bukovina State Medical University
Chernivsti, 58000, Ukraine

Abstract. We investigate the statistical polarization parameters of biological tissue histological section images with different morphological structure. First we outline the results of polarization coordinate mapping and analysis of the statistics of the first to fourth orders of biological tissue image polarization azimuth and ellipticities. Second, we study the statistics of the first to fourth orders of coordinate distributions of the complex degree of mutual polarization (CDMP) of biological tissue images. Finally, we consider the diagnostic possibilities of investigating 2-D distributions of CDMP of images that correspond to physiologically normal and degeneratively and/or dystrophycally changed biological tissues that are being analyzed. [DOI: 10.1117/1.2148251]

Keywords: complex degree of mutual polarization; biological tissue; polarization; statistical moments.

Paper 05119R received May 14, 2005; revised manuscript received Jul. 8, 2005; accepted for publication Jul. 18, 2005; published online Jan. 5, 2006.

1 Introduction

Historically optical methods for researching biological tissue (BT) structure can be divided into three main groups:

1. Spectrophotometric methods[1–3] based on the analysis of spatial (r) [temporal (τ)] changes of field intensity of radiation scattered by BT

2. Polarization methods using the coherency matrix of complex amplitude[4–6] $\{\mathbf{K}(r,\tau)\}$:

$$\mathbf{K}(r,\tau)=\left\|\begin{array}{cc}\langle E_x(r,\tau)E_x^*(r,\tau)\rangle & \langle E_x(r,\tau)E_y^*(r,\tau)\rangle\\ \langle E_x^*(r,\tau)E_y(r,\tau)\rangle & \langle E_y(r,\tau)E_y^*(r,\tau)\rangle\end{array}\right\|, \quad (1)$$

and based on the analysis of polarization degree $P(r)$ as correlation function between complex orthogonal components of electromagnetic oscillations E_x and E_y in that of point (r) of the scattered radiation field:[7]

$$P(r)=\left\{1-\frac{4\left|\left[\langle E_x(r,\tau)E_x^*(r,\tau)\rangle\langle E_y(r,\tau)E_y^*(r,\tau)\rangle-\langle E_x(r,\tau)E_y^*(r,\tau)\rangle\langle E_y(r,\tau)E_x^*(r,\tau)\rangle\right]\right|}{\left[\langle E_x(r,\tau)E_x^*(r,\tau)\rangle+\langle E_y(r,\tau)E_y^*(r,\tau)\rangle\right]^2}\right\}. \quad (2)$$

3. Correlation methods based on the analysis of correlation degree J between parallel polarization components $E_x(r_1)$, $E_x(r_2)$ of light oscillations in different points of object field[7,8] (r_1,r_2):

$$J=\frac{\langle E_x(r_1,\tau)E_x^*(r_2,\tau)\rangle-\langle E_x^*(r_1,\tau)E_x(r_2,\tau)\rangle}{\langle E_x(r_1,\tau)E_x^*(r_2,\tau)\rangle+\langle E_x^*(r_1,\tau)E_x(r_2,\tau)\rangle}. \quad (3)$$

Real-object BT fields, including their images, have a change of both polarization and correlation characteristics.[9] In the case of single scattering, there is an unequivocal interconnection between the morphological structure of BT histological section and polarization characteristics of an image. To analyze these fields a new methodological approach was proposed,[10–12] which is based on the generalization of coherence matrix $\{\mathbf{K}(r,\tau)\}$ by two-point (r_1,r_2) polarization coherence matrix $\{\mathbf{\Phi}(r_1,r_2,\tau)\}$:

$$\mathbf{K}(r,\tau)\Rightarrow\Phi(r_1,r_2,\tau), \quad (4)$$

$$\left\|\begin{array}{cc}\langle E_x(r,\tau)E_x^*(r,\tau)\rangle & \langle E_x(r,\tau)E_y^*(r,\tau)\rangle\\ \langle E_x^*(r,\tau)E_y(r,\tau)\rangle & \langle E_y(r,\tau)E_y^*(r,\tau)\rangle\end{array}\right\| \Rightarrow \left\|\begin{array}{cc}\langle E_x(r_1,\tau)E_x^*(r_2,\tau)\rangle & \langle E_x(r_1,\tau)E_y^*(r_2,\tau)\rangle\\ \langle E_x^*(r_1,\tau)E_y(r_2,\tau)\rangle & \langle E_y(r_1,\tau)E_y^*(r_2,\tau)\rangle\end{array}\right\|. \quad (5)$$

According to Eq. (5) the main parameter determining correlation between differently polarized points (r_1,r_2) of object

Address all correspondence to Alexander Ushenko, Correlation Optics, Chernivtsi National University, 2 Kotsyubinsky Str., Chernivtsi, Chernivtsi 58012, Ukraine. Tel: +3802372244730. Fax: +3802372244730. E-mail: ushenko-bio@itf.cv.ukrtel.net

1083-3668/2005/10(6)/064025/12/$22.00 © 2005 SPIE

field with intensities $I(r_1,\tau)$ and $I(r_2,\tau)$ is considered to be complex degree of mutual polarization[13,14] (CDMP) $V^2(r_1,r_2,\tau)$. The latter is written in the following form

$$V^2(r_1,r_2,\tau)=4\frac{v_1^2+v_2^2+v_3^2}{I(r_1,\tau)I(r_2,\tau)}, \tag{6}$$

where coefficients v_i are defined by relations

$$v_1=\frac{\langle E_x(r_1,\tau)E_x^*(r_2,\tau)\rangle-\langle E_y(r_1,\tau)E_y^*(r_2,\tau)\rangle}{2},$$

$$v_2=\frac{\langle E_x(r_1,\tau)E_y^*(r_2,\tau)\rangle-\langle E_y(r_1,\tau)E_x^*(r_2,\tau)\rangle}{2},$$

$$v_3=i\frac{\langle E_x(r_1,\tau)E_y^*(r_2,\tau)\rangle-\langle E_y(r_1,\tau)E_x^*(r_2,\tau)\rangle}{2}, \tag{7}$$

and have a meaning of value differences of interference pattern visibility from points r_1 and r_2, which are measured through differently oriented polarization filter (v_1 are axis rotation angles of the analyzer 0, 90 deg; v_2 are 45, 135 deg; and v_3 are right or left circulation).

Let us consider two differently polarized laser oscillations in points r_1, r_2 of a BT image:

$$\begin{cases} E_x(r_1)+E_y(r_1)\exp[-i\delta_1(r_1)], \\ E_x(r_2)+E_y(r_2)\exp[-i\delta_2(r_2)]. \end{cases} \tag{8}$$

Here $\delta_1(r_1)$ and $\delta_2(r_2)$ are phase shifts between orthogonal components of complex amplitudes E_x and E_y at points r_1 and r_2.

For the situation of completely correlated laser BT image a generalized coherence matrix, Eq. (1) takes the following form:

$$\mathbf{\Phi}(r_1,r_2)=\left\| \begin{matrix} E_x(r_1)E_x^*(r_2) & E_x(r_1)E_y^*(r_2) \\ E_x^*(r_1)E_y(r_2) & E_y(r_1)E_y^*(r_2) \end{matrix} \right\|. \tag{9}$$

Taking into account Eq. (8), the operator of Eq. (9) can be rewritten in the following way:

$$\mathbf{\Phi}(r_1,r_2)=\left\| \begin{matrix} E_x(r_1)E_x(r_2) & E_x(r_1)E_y(r_2)\exp[i\delta(r_2)] \\ E_y(r_1)E_x(r_2)\exp[i\delta(r_1)] & E_y(r_1)E_y(r_2) \end{matrix} \right\|. \tag{10}$$

Based on Eq. (10) and taking into account Eqs. (5)–(7), one can show that CDMP for two image points considered is described by the relation

$$V^2(r_1,r_2)=\frac{[E_x(r_1)E_x(r_2)-E_y(r_1)E_y(r_2)]^2+4E_x(r_1)E_x(r_2)E_y(r_1)E_y(r_2)\exp\{i[\delta_2(r_2)-\delta_1(r_1)]\}}{[E_x^2(r_1)+E_y^2(r_1)][E_x^2(r_2)+E_y^2(r_2)]}. \tag{11}$$

Currently only several publications[15–18] dedicated to problems of CDMP direct measurement of statistical fields of scattered laser radiation are known. This approach is urgent in biomedical optics concerned with processing of coherent polarization-inhomogeneous biotissue images.[19]

This paper deals with the elaboration of polarization measuring of 2-D distributions of CDMP of BT images for searching their interrelationship with orientation morphological structure of birefringent architectonic nets during early, preclinical diagnostics of their physiological state.

2 Theoretical Modeling

2.1 *Polarization Maps (PMs) of Biotissue Images*

The analysis of the formation of a BT image PM is based on an approach that enables the morphological presentation of these bio-objects by using two-component amorphous **A** and crystalline **C** matrices, and their optical properties can be described by the following Jones operators:[20]

$$\mathbf{A}=\left\| \begin{matrix} \exp(-\chi l) & 0 \\ 0 & \exp(-\chi l) \end{matrix} \right\|, \tag{12}$$

$$\mathbf{C}=\left\| \begin{matrix} \cos^2\rho+\sin^2\rho\exp(-i\delta) & \cos\rho\sin\rho[1-\exp(-i\delta)] \\ \cos\rho\sin\rho[1-\exp(-i\delta)] & \sin^2\rho+\cos^2\rho\exp(-i\delta) \end{matrix} \right\|, \tag{13}$$

where χ is the coefficient of laser radiation absorption by the BT amorphous layer with geometrical thickness l; and ρ is package direction of birefringent fibrils in the plane of BT sample, the substance of which (fibrils) introduces phase-shift δ between orthogonal polarization components E_{0x} and E_{0y} of illuminating laser beam.

According to Eqs. (12) and (13), the amplitude-phase structure of imaging amorphous and crystalline BT components can be described analytically by the following matrix equations

$$\begin{bmatrix} E_x^A(r_A) \\ E_y^A(r_A) \end{bmatrix} = \mathbf{A}\begin{pmatrix} E_{0x} \\ E_{0y} \end{pmatrix}, \tag{14}$$

$$\begin{bmatrix} E_x^C(r_C) \\ E_y^C(r_C) \end{bmatrix} = \mathbf{C}\begin{pmatrix} E_{0x} \\ E_{0y} \end{pmatrix}, \tag{15}$$

where $[E_x^A(r_A), E_y^A(r_A)]$ and $[E_x^C(r_C), E_y^C(r_C)]$ are complex amplitudes of orthogonally polarized laser oscillations at points r_A of amorphous and r_C of the crystalline (architectonic[20]) constituent parts of BT image.

For simplicity, let us consider the formation of BT image polarization structure under its probing by linearly polarized laser beam with azimuth $\alpha=0$ deg relatively to inclination plane:

$$\begin{pmatrix} E_{0x} \\ E_{0y} \end{pmatrix} \Rightarrow \begin{pmatrix} E_{0x} \\ 0 \end{pmatrix}. \tag{16}$$

Taking into account Eq. (16) relations (14) and (15) are rewritten as follows:

$$E_x^A(r) = E_{0x}\exp(-\chi l)$$

$$E_y^A(r) = 0, \tag{17}$$

$$E_x^C(r) = E_{0x}\{\cos^2\rho(r) + \sin^2\rho(r)\exp[-i\delta(r)]\},$$

$$E_y^C(r) = E_{0x}(\cos\rho(r)\sin\rho(r)\{1-\exp[-i\delta(r)]\}). \tag{18}$$

To determine the local states of light oscillation polarization at the points of a BT image let us write their corresponding coherence matrices of amorphous $\mathbf{K}^A(r)$ and crystalline $\mathbf{K}^C(r)$ constituent parts:

$$\mathbf{K}^A(r) = E_{0x}^A\left\|\begin{matrix}\exp(-\chi l) & 0\\ 0 & 0\end{matrix}\right\|, \tag{19}$$

$$\mathbf{K}^C(r) = \left\|\begin{matrix}E_x^C(r)E_x^{*C}(r) & E_x^C(r)E_y^{*C}(r)\\ E_x^{*C}(r)E_y^C(r) & E_y^C(r)E_y^{*C}(r)\end{matrix}\right\|. \tag{20}$$

According to Eqs. (19) and (20), the coordinate distribution of azimuth $\alpha(r)$ and ellipticity $\beta(r)$ polarization states of a BT image are represented by two types of PM—polarization homogeneous,

$$\begin{cases}\alpha^A(r) = 0 \text{ deg}\\ \beta^A(r) = 0 \text{ deg},\end{cases} \tag{21}$$

and polarization inhomogeneous ones,

$$\begin{cases}\alpha^C(r) = 0.5\arctan\left[\dfrac{E_x^C(r)E_y^{*C}(r) - E_x^{*C}(r)E_y^C(r)}{E_x^C(r)E_x^{*C}(r) - E_y^C(r)E_y^{*C}(r)}\right],\\ \beta^C(r) = 0.5\arcsin\left\{\dfrac{i[E_x^C(r)E_y^{*C}(r) - E_x^{*C}(r)E_y^C(r)]}{(q_1+q_2+q_3)^{1/2}}\right\},\end{cases} \tag{22}$$

where

$$q_1 = [E_x^C(r)E_x^{*C}(r) - E_y^C(r)E_y^{*C}(r)]^2,$$

$$q_2 = [E_x^C(r)E_x^{*C}(r) - E_y^{*C}(r)E_y^C(r)]^2,$$

$$q_3 = i[E_x^C(r)E_y^{*C}(r) - E_x^{*C}(r)E_y^C(r)]^2. \tag{23}$$

Here $r \equiv \begin{pmatrix} r_1,\ldots,r_m \\ \vdots \\ r_n,\ldots,r_m \end{pmatrix}$ is the totality of BT image coordinates defined by the pixel amount of registering area CCD camera.

2.2 *Complex Degree of Mutual Polarization of BT Images*

The CDMP relation [Eq. (11)] analysis shows that the values of local phase shifts $\delta_1(r_1)$ and $\delta_2(r_2)$ are concerned with parameters $\alpha\begin{pmatrix} r_1,\ldots,r_m \\ \vdots \\ r_n,\ldots,r_m \end{pmatrix}$ and $\beta\begin{pmatrix} r_1,\ldots,r_m \\ \vdots \\ r_n,\ldots,r_m \end{pmatrix}$ of polarization map of BT image by the following relations:

$$\delta(r_1) = \arctan\left[\frac{\tan 2\beta(r_1)}{\tan\alpha(r_1)}\right],$$

$$\delta(r_2) = \arctan\left[\frac{\tan 2\beta(r_2)}{\tan\alpha(r_2)}\right]. \tag{24}$$

The analysis of Eqs. (8)–(10) and Eq. (24) shows that the range of the CDMP $V^2(r_1, r_2)$ change turns out to be wide enough for different polarization states of light oscillations $E(r_1)$ and $E(r_2)$ at points (r_1, r_2), and it is situated within 0.0 (orthogonal states) and 1.0 (collinear states).

The significant cases of the correlation interconnections between the different polarization states (collinear and orthogonal, linear with different azimuths, linear and circular, etc.) at the points (r_1, r_2) are shown in the Table 1.

Thus, having the information on coordinate distribution of parameters $\alpha(r)$, $\beta(r)$, $E_x(r)$, and $E_y(r)$ one can define 2-D distributions of CDMP of BT images with a random discretization interval Δr_i:

$$\Delta r_1 = r_{n+1} - r_n,$$

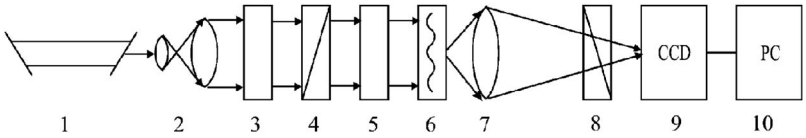

Fig. 1 Optical scheme for measuring PCMs of BT images, where 1, He–Ne laser; 2, collimator; 3 and 5, quarter-wave plates; 4 and 8, polarizer and analyzer, respectively; 6, object of investigation; 7, microobjective; 9, CCD camera; and 10, personal computer.

Table 1 Complex degree of mutual polarization of different types light oscillations.

$E(r_1)$	$E(r_2)$	$V^2(r_1, r_2)$
$E_x(r_1)$; $E_x(r_1)+E_y(r_1)\exp(i\delta)$	$E_x(r_2)$; $E_x(r_2)+E_y(r_2)\exp(i\delta)$	1
$E_x(r_1)$	$E_x(r_2)+E_y(r_2)$	$\frac{E_x^2(r_2)}{E_x^2(r_2)+E_y^2(r_2)}$
$E_x(r_1)$	$E_x(r_2)+iE_y(r_2)$	0.5
$E_x(r_1)$; $E_x(r_1)+E_y(r_1)\exp(i\delta)$	$E_y(r_2)$; $E_x(r_2)-E_y(r_2)\exp(i\delta)$	0

$$\Delta r_2 = r_{n+2} - r_n,$$

$$\vdots$$

$$\Delta r_k = r_{n+k} - r_n. \tag{25}$$

3 Experimental Measuring of BT Polarization-Correlation Maps (PCMs)

The optical scheme of measuring BT PCM is presented in Fig. 1. Illumination was realized by collimated ($\varnothing = 10^4$ μm) He–Ne laser beam ($\lambda = 0.6328$ μm, $W = 5.0$ mW). Polarization illuminator consisted of quarter-wave plates (3) and (5) and polarizer (4) forms illuminating beam with the range of azimuth 0 deg $\leqslant \alpha_0 \leqslant$ 180 deg and with the range of ellipticity 0 deg $\leqslant \beta_0 \leqslant$ 90 deg of polarization.

Polarization BT images with the help of microscope objective (7) were projected into the plane of light-sensitive area (800×600 pixels) of CCD camera (9) provided with measuring range of structural BT elements for the following scales 2 to 2000 μm.

The experimental conditions were designed to eliminate spatial-angular aperture filtration under BT image formation. This was provided by correspondence of indicatrix angular characteristics of light scattering by BT samples ($\Omega_{BT} \approx 16$ deg) and microscope objective angular aperture ($\Delta\omega = 20$ deg). Here Ω_{BT} is the plane angle of cones where there is concentrated 98% of the total energy of scattered radiation. The analysis of BT images was realized by using polarizer (8).

The methodology of defining BT images polarization-correlation structure consists in the following sequence of actions:

1. By using CCD (9) [without analyzer (8)] one can measure an array of intensities of BT image $I\begin{pmatrix} r_1,\ldots,r_m \\ \vdots \\ r_n,\ldots,r_m \end{pmatrix}$.

2. Then by setting up the analyzer (9), the optical axis of which is sequentially oriented at angles $\Theta = 0$ deg and $\Theta = 90$ deg, one can measure arrays of intensities $I^{(0)}\begin{pmatrix} r_1,\ldots,r_m \\ \vdots \\ r_n,\ldots,r_m \end{pmatrix}$ and $I^{(90)}\begin{pmatrix} r_1,\ldots,r_m \\ \vdots \\ r_n,\ldots,r_m \end{pmatrix}$.

3. By rotating passage axis Θ of analyzer within $\Theta = 0$ to 180-deg one can define arrays of minimum and maximum intensity levels $I_{\min}\begin{pmatrix} r_1,\ldots,r_m \\ \vdots \\ r_n,\ldots,r_m \end{pmatrix}$ and $I_{\max}\begin{pmatrix} r_1,\ldots,r_m \\ \vdots \\ r_n,\ldots,r_m \end{pmatrix}$ of laser image for each individual pixel (m,n) of CCD camera and their corresponding rotation angles $\Theta\begin{pmatrix} r_1,\ldots,r_m \\ \vdots \\ r_n,\ldots,r_m \end{pmatrix}\left[I\begin{pmatrix} r_1,\ldots,r_m \\ \vdots \\ r_n,\ldots,r_m \end{pmatrix} \equiv I_{\min}\right]$.

4. Then calculate PM of BT image by using the following relationship:

$$\alpha\begin{pmatrix} r_1,\ldots,r_m \\ \vdots \\ r_n,\ldots,r_m \end{pmatrix} = \Theta[I(r) \equiv I_{\min}] - \frac{\pi}{2},$$

$$\beta\begin{pmatrix} r_1,\ldots,r_m \\ \vdots \\ r_n,\ldots,r_m \end{pmatrix} = \arctan\frac{I(r)_{\min}}{I(r)_{\max}}. \tag{26}$$

5. The coordinate distribution of CDMP of BT images are calculated using the following algorithm:

$$V^2(r_{n+k}, r_n) = \frac{\{[I^{(0)}(r_{n+k})I^{(0)}(r_n)]^{1/2} - [I^{(90)}(r_{n+k})I^{(90)}(r_n)]^{1/2}\}^2}{I(r_{n+k})I(r_n)} + \frac{4[I^{(0)}(r_{n+k})I^{(90)}(r_{n+k})I^{(0)}(r_n)I^{(90)}(r_n)]^{1/2}\cos[\delta_{n+k}(r_{n+k}) - \delta_n(r_n)]}{I(r_{n+k})I(r_n)}. \tag{27}$$

4 Characteristics of Research Objects

As research objects are "optically thin" ($\tau \leqslant 0.1$) histological BT cuts of different morphological structure:

1. Muscular tissue (myocardium)—MT [Figs. 2(a) and 2(b)],
2. Kidney tissue—KT [Figs. 2(c) and 2(d)],
3. Spleen tissue—ST [Figs. 2(e) and 2(f)].

The research objects chosen have the similar optical anisotropic components with birefringence index $\Delta n \approx 1.5 \times 10^{-3}$ visualized in crossed polarizer and analyzer [Figs. 2(b), 2(d), and 2(f)].

The morphological architectonic structure of such a BT is different. MT is formed by "quasiordered" bundles of birefringent myosin bundles [Fig. 2(b)]. KT architectonics is

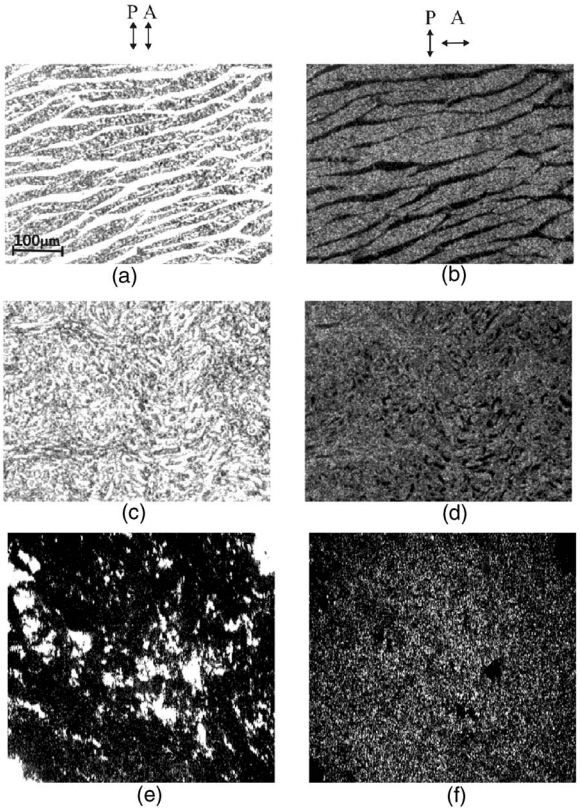

Fig. 2 Images of different types of BTs: (a) and (b) MT, (c) and (d) KT, and (e) and (f) ST in parallel (left column) and crossed (right column) polarizer (P) and analyzer (A). The arrows depict the orientation of the optical axes of both polarizer (A) and analyzer (B), respectively.

made by collagen fibers oriented chaotically [Fig. 2(d)]. ST includes "island" inclusions of anisotropic collagen [Fig. 2(f)].

A similar sample selection provides the possibility to do the analysis of the influence of orientation architectonics peculiarities of physiologically different BT in a PM speckle-image structure.

5 Analysis and Discussion of Experimental Data

The experimental part of research contains the following data:

1. PMs $\alpha\binom{r_1,\ldots,r_m}{r_n,\ldots,r_m}$ and $\beta\binom{r_1,\ldots,r_m}{r_n,\ldots,r_m}$ of all types of BT images [Figs. 3(a), 3(b), 4(a), 4(b), 5(a), and 5(b)]
2. Probability distributions W of azimuth $\alpha(r)$ and ellipticity $\beta(r)$ polarization values and their corresponding statistical moments of the first to fourth orders (Figs. 3(c), 3(d), 4(c), 4(d), 5(c), and 5(d)); Table 2;
3. PCMs $[2DV^2(\Delta r_i)]$ of BT images with different intervals of discretization Δr_i [Figs. 6(a), 7(a), and 8(a)].
4. Probability distributions $Q[V^2(\Delta r_i)]$ and corresponding statistical moments of first to fourth orders [Figs. 6(b), 7(b), and 8(b)] and Table 3.

5.1 *PMs*

The coordinate structure of PM of MT images [Figs. 3(a) and 3(b)] is considered to be ensembles of large-scale (100 to 200-μm) monopolarized $[\{\alpha(r);\beta(r)\}\approx\text{const}]$ regions (polarization domains). The areas of similar polarization for KT images [Figs. 4(a) and 4(b)] are more small-scale (25 to 100 μm) and have a rather chaotic form. PM of ST (Fig. 5(a) and 5(b)) are formed by polarized parts of small sizes (5 to 20 μm) and located equiprobable enough in the plane of laser image.

Histograms $W(\alpha)$ and $W(\beta)$ [Figs. 3(c), 3(d), 4(c), 4(d), 5(c), and 5(d)] characterize the peculiarities of probability distributions of polarization parameters $\{\alpha(r);\beta(r)\}$ of BT images. It is peculiar to MT to have dependency extremes of $W(\alpha)$ and $W(\beta)$ expressed distinctly [Figs. 3(c) and 3(d)]. They point out to statistical prevalence of a certain polarization state of its architectonic net in laser image. Histograms of PM of KT images [Figs. 4(c) and 4(d)] are formed by a series of local extremes in a wider range of value change of polarization parameters $\{\alpha(r);\beta(r)\}$. Probability polarization structure of ST image [Figs. 5(c) and 5(d)] is made by superposition of two components: polarization-homogeneous component, coinciding with polarization state of illuminating beam ($\alpha_0=0$ deg, $\beta_0=0$ deg) and polarization-inhomogeneous ones. The first PM component is characterized by histogram extremes $W(\alpha)$ and $W(\beta)$ expressed distinctly; the second one, by the totality of local extremes of a small value.

Actually dependencies $W(\alpha)$ and $W(\beta)$ are characterized by the totality of statistical moments of first to fourth orders of azimuths and ellipticities values, and they are calculated using the following relationship:

$$M_{\alpha,\beta}=\frac{1}{N}\sum_{i=1}^{N}|z_i|,$$

$$\sigma_{\alpha,\beta}=\left(\frac{1}{N}\sum_{i=1}^{N}z_i^2\right),$$

$$A_{\alpha,\beta}=\frac{1}{\sigma_S^3}\frac{1}{N}\sum_{i=1}^{N}z_i^3,$$

$$E_{\alpha,\beta}=\frac{1}{\sigma_S^2}\frac{1}{N}\sum_{i=1}^{N}z_i^4, \tag{28}$$

where $N=m\times n$—the overall number of CCD camera pixels, and z_i corresponds to α_i or β_i values.

The quantitative values of parameters Eq. (28) averaged at statistically reliable amount of all types of BT samples are shown in Table 2.

The researched PM structure of different types of BT can concern the following peculiarities of morphological structure of their architectonics. The structures transforming laser radiation polarization for MT are large-scale domains of "mono-oriented" myosin fibers. According to Eqs. (22) and (23) coordinate distribution of azimuth $\alpha\binom{r_1,\ldots,r_m}{r_n,\ldots,r_m}$ and ellipticity $\beta\binom{r_1,\ldots,r_m}{r_n,\ldots,r_m}$ polarization turns to be homogeneous within

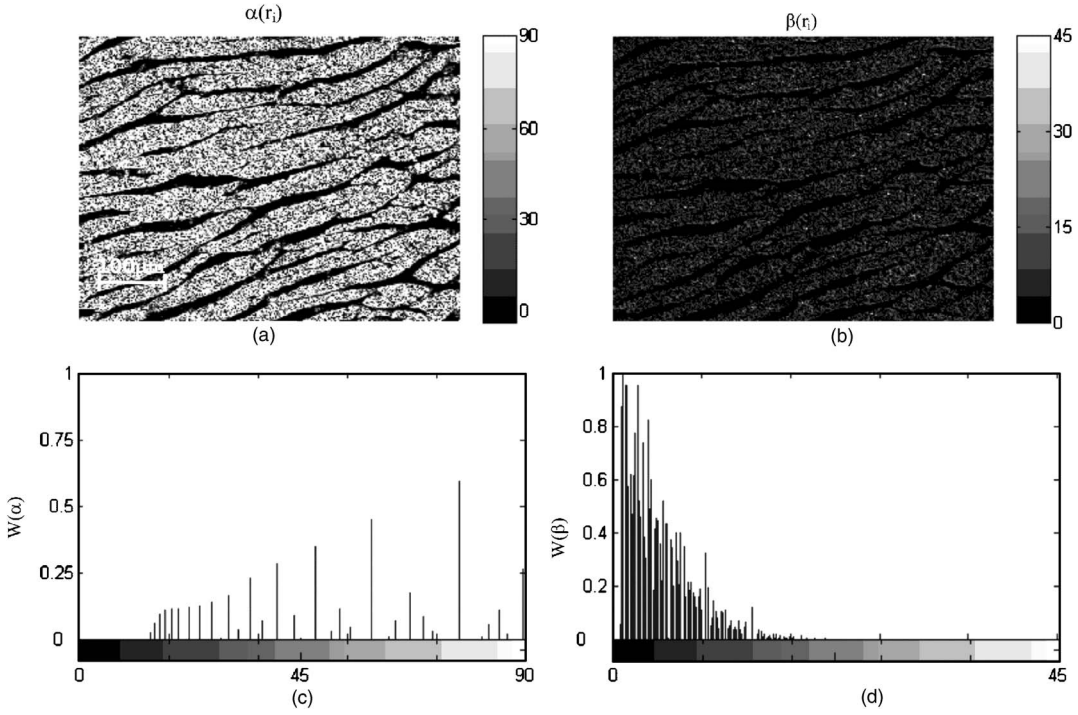

Fig. 3 PMs of (a) azimuth and (b) ellipticities of MT images and (c) and (d) their probability structure.

such domains as $\rho, \delta(\begin{smallmatrix} r_1,\ldots,r_k \\ \vdots \\ r_g,\ldots,r_q \end{smallmatrix})_{1\leqslant l,k,g,q\leqslant m,n} \approx \text{const}$ [Figs. 3(a) and 3(b)] and corresponding histograms $W(\alpha)$, $W(\beta)$ have expressed extremes [Figs. 3(c) and 3(d)].

A wide spectrum of angles between polarization azimuth of illuminating beam α_0 and local angles ρ in case of KT architectonic net is realized, which is formed by collagen fibers oriented chaotically. Hence, regional areas of identical polarization decrease [Figs. 4(a) and 4(b)], and their corresponding histograms can be represented as sets of a great number of local extremes [Figs. 4(c) and 4(d)].

The ST anisotropic component does not have a distinct fibrous, fibrillar structure. Therefore, the polarization-inhomogeneous component of its speckle-images is formed by values of polarization of azimuths and ellipticities distributed equiprobable enough [Figs. 5(a) and 5(b)], the probabilities of which are one order less than polarization parameters of illuminating laser beam [Figs. 5(c) and 5(d)].

The information on statistical moments of the first to fourth orders of the distribution of $W(\alpha)$ and $W(\beta)$ of different tissues speckle-images help us to determine the following:

$$M_{\alpha,\beta}(\mathrm{MT}) \geqslant M_{\alpha,\beta}(\mathrm{KT}) \geqslant M_{\alpha,\beta}(\mathrm{ST}),$$

$$\sigma_{\alpha,\beta}(\mathrm{MT}) \geqslant \sigma_{\alpha,\beta}(\mathrm{KT}) \geqslant \sigma_{\alpha,\beta}(\mathrm{ST}),$$

$$A_{\alpha,\beta}(\mathrm{MT}) \geqslant A_{\alpha,\beta}(\mathrm{KT}) \geqslant A_{\alpha,\beta}(\mathrm{ST}),$$

Table 2 Statistics of the first to fourth orders of polarization states of BT images.

MT (37 samples)				KT (34 samples)				ST (35 samples)			
$\alpha(r_i)$		$\beta(r_i)$		$\alpha(r_i)$		$\beta(r_i)$		$\alpha(r_i)$		$\beta(r_i)$	
M_α	0.38± 3%	M_β	0.24± 4%	M_α	0.29± 2%	M_β	0.18± 4%	M_α	0.11± 3%	M_β	0.08± 5%
σ_α	0.25± 4%	α_β	0.21± 5%	σ_α	0.18± 4%	σ_β	0.16± 6%	σ_α	0.06± 3%	σ_β	0.05± 7%
A_α	93.8± 9%	A_β	89.7± 11%	A_α	79.4± 7%	A_β	68.3± 12%	A_α	20.4± 14%	A_β	16.1± 17%
E_α	981.6± 16%	E_β	832.0 ±19%	E_α	682.7 ±14%	E_β	574.2 ±18%	E_α	11.4± 9%	E_β	8.25± 10%

Table 3 Statistics of the first to fourth orders of CDMP of BT images.

MT (37 samples)		KT (34 samples)		ST (35 samples)	
M_{V2}	0.18±6%	M_{V2}	0.24±4%	M_{V2}	0.03±7%
σ_{V2}	0.11±8%	σ_{V2}	0.18±6%	σ_{V2}	0.02±9%
A_{V2}	67.4±10%	A_{V2}	259.3±9%	A_{V2}	17.4±12%
E_{V2}	324.2±14%	E_{V2}	874.9±11%	E_{V2}	26.9±15%

$$E_{\alpha,\beta}(\mathrm{MT}) \geqslant E_{\alpha,\beta}(\mathrm{KT}) \geqslant E_{\alpha,\beta}(\mathrm{ST}). \tag{29}$$

It is clear that the more the probability distributions of optical-geometrical parameters of architectonic nets deviate from the statistical (equiprobable or normal law) character to a stochastic and self-similar one, the greater become values of corresponding statistical moments of polarization parameters of BT images.

5.2 *Polarization-Correlation Maps*

Distributions of $2D[V^2(\Delta r_i)]$ of MT images obtained for $\Delta r_i = 1$ pixel are mainly formed by large-scale (25 to 100 μm) regions [Fig. 6(a)] with maximum correlated polarization states ($V^2(\Delta r_i) \to 1$). Statistically, this points out to the basic histogram $\{Q[V^2(\Delta r_i)]\}$ extremum [Fig. 6(b)]. Along with this fact $2D[V^2(\Delta r_i)]$ have regions where the CDMP value changes within a wide range $[0 \leqslant V^2(\Delta r_i) \leqslant 1]$, which has corresponding additional extremes on the histogram $Q[V^2(\Delta r_i)]$.

Except for the areas of maximum polarization correlation, all-scale (10 to 30 μm) regions, where CDMP value changes within a wide range $[0 \leqslant V^2(\Delta r_i) \leqslant 1]$ [Fig. 7(a)], form a distribution of $2D[V^2(\Delta r_i)]$ of the MT image. The corresponding histograms $Q[V^2(\Delta r_i)]$ also include the totality of considerably equiprobable extrema for what are actually whole range of value change of CDMP of KT images [Fig. 7(b)].

The correlation structure of polarization states of speckle-images points out to essential prevalence of their polarization homogeneous component. Distributions of $2D[V^2(\Delta r_i)]$ [Fig. 8(a)] are considered to be the totality of regions with the extreme CDMP value $V^2(\Delta r_i) \to 1$. The histogram [Fig. 8(b)] by its structure is close to a δ functions of the form

$$Q[V^2(\Delta r_i)] = \begin{cases} 1[V^2(\Delta r_i) = 1] \\ \to 0[V^2(\Delta r_i) \neq 1]. \end{cases}$$

The totality of statistical moments of the first to fourth value orders $Q[V^2(\Delta r_i)]$ of images of all types of BT are shown in Table 3.

The researched structure of $2D[V^2(\Delta r_i)]$ BT images closely concerns the different morphological structures of their architectonics. The package order of MT myosin fibrils

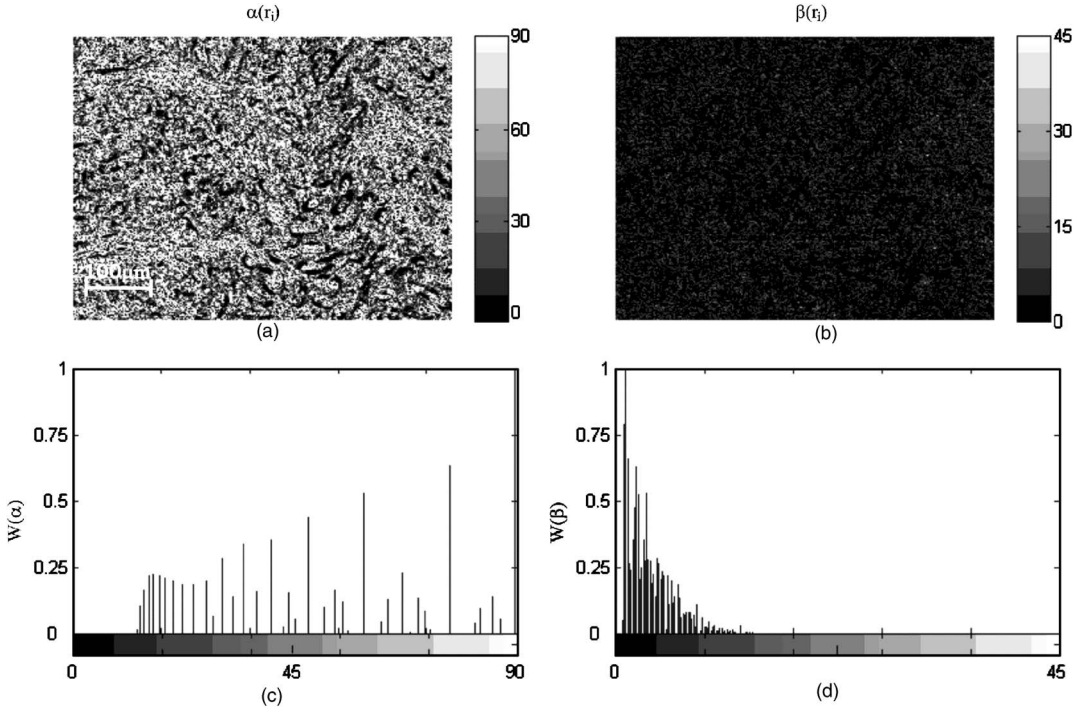

Fig. 4 Coordinate and probability distributions of (a) and (c) azimuths and (b) and (d) of the polarization states of points of kidney tissue image.

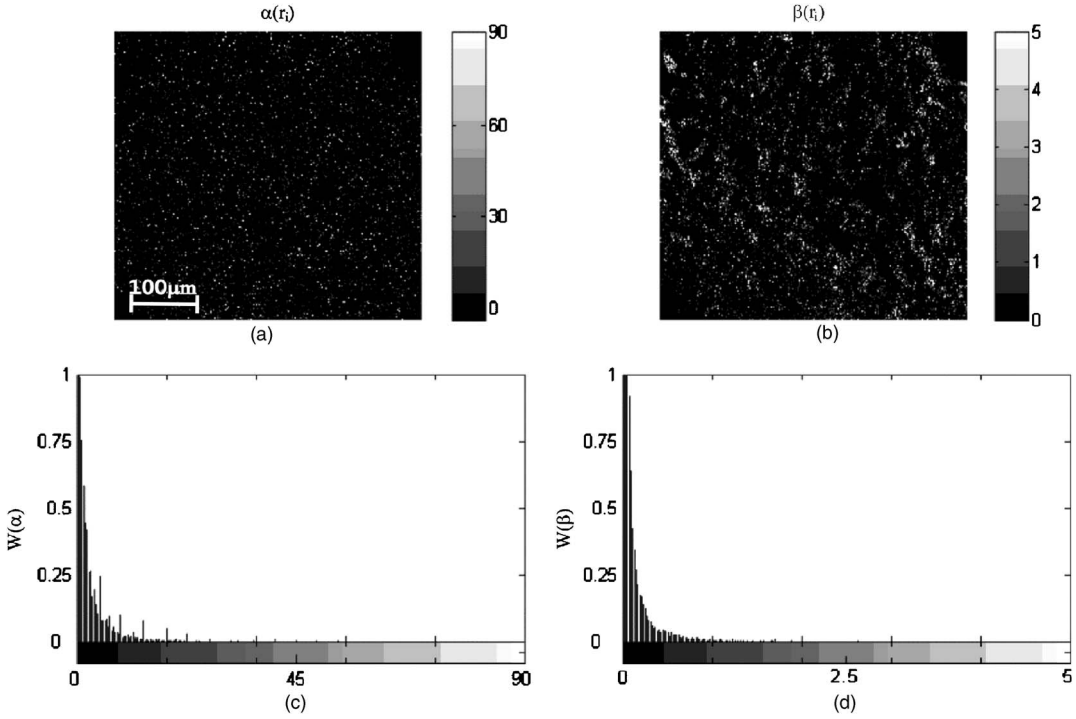

Fig. 5 PMs of (a) azimuth and (b) ellipticities of ST image and (c) and (d) their probability structures, respectively.

within considerably large geometrical domains according to Eqs. (11), (22), and (23) conditions the high degree of correlation identity $[V^2(\Delta r_i) \rightarrow 1]$ of polarization states of corresponding image points. The transition to other domains (parts with a different orientation architectonic structure) is accompanied with CDMP value decrease of the given image parts. However, within the domain the degree of mutual polarization of MT image points increases extremely again [Fig. 6(a)].

There is a more dynamic value change $V^2(\Delta r_i)$ for image points of different parts of architectonic net in case of a 2-D distribution of the CDMP of images of a collagen net that is oriented chaotically. Therefore, along with the main maximum statistical distributions $Q[V^2(\Delta r_i)]$ are formed by considerably equiprobable extremes [Fig. 7(b)], which are conditioned by a variety of KT architectonics orientation structure and by the decrease of its self-similar geometrical sizes as well [Fig. 7(a)].

The structure of $2D[V^2(\Delta r_i)]$ ST images represents the high correlation interrelation between points' polarization states of a completely polarization-homogeneous image [Figs. 8(a) and 8(b)].

A comparative analysis of statistical moments' values of the first to fourth orders of parameter $V^2(\Delta r_i)$ shows

$$M_{V^2}(\mathrm{MT}) \geqslant M_{V^2}(\mathrm{KT}) \geqslant M_{V^2}(\mathrm{ST}),$$

$$\sigma_{V^2}(\mathrm{MT}) \geqslant \sigma_{V^2}(\mathrm{KT}) \geqslant \sigma_{V^2}(\mathrm{ST}),$$

$$A_{V^2}(\mathrm{MT}) \geqslant A_{V^2}(\mathrm{KT}) \geqslant A_{V^2}(\mathrm{ST}),$$

$$E_{V^2}(\mathrm{MT}) \geqslant E_{V^2}(\mathrm{KT}) \geqslant E_{V^2}(\mathrm{ST}). \qquad (30)$$

A comparative analysis Eq. (30) and Eq. (29) determines the large sensitivity (within 2 to 5 times) to the orientation structure peculiarities of architectonic nets of statistical moments of third and fourth orders of parameter $V^2(\Delta r_i)$ in comparison with analogous parameters of polarization maps $\alpha\begin{pmatrix} r_1,\ldots,r_m \\ \vdots \\ r_n,\ldots,r_m \end{pmatrix}$ and $\beta\begin{pmatrix} r_1,\ldots,r_m \\ \vdots \\ r_n,\ldots,r_m \end{pmatrix}$ of BT images. This is why the investigation of possibility of using the polarization-correlation analysis of BT images during the diagnostics of their physiological state, which is connected with architectonic nets structure changes, is topical.

6 Pathological Changes Diagnostics Using Complex Degree of Mutual Polarization of BT Images

This part of the paper deals with searching for an interconnection between the coordinate structure CDMP of BT images and the optical-geometrical parameters of their physiologically normal and pathologically changed birefringent architectonics nets.

The main idea consists in the fact that the values of $\alpha(r)$, $\beta(r)$, $E_x(r)$, and $E_y(r)$ at every point of the BT image appear to be connected with orientational $\rho(r)$ and phase $\delta(r)$ parameters of its architectonics [Eqs. (11), (14), and (22)]:

$$\alpha(r) = 0.5 \arctan\left[\frac{\sin 4\rho(r)\sin^2 0.5\delta(r)}{\cos^2 2\rho(r) + \sin^2 2\rho(r)\cos\,\delta(r)}\right],$$

$$\beta(r) = 0.5 \arcsin\left[\frac{\tan 2\rho(r)}{\sin\,\delta(r)}\right], \qquad (31)$$

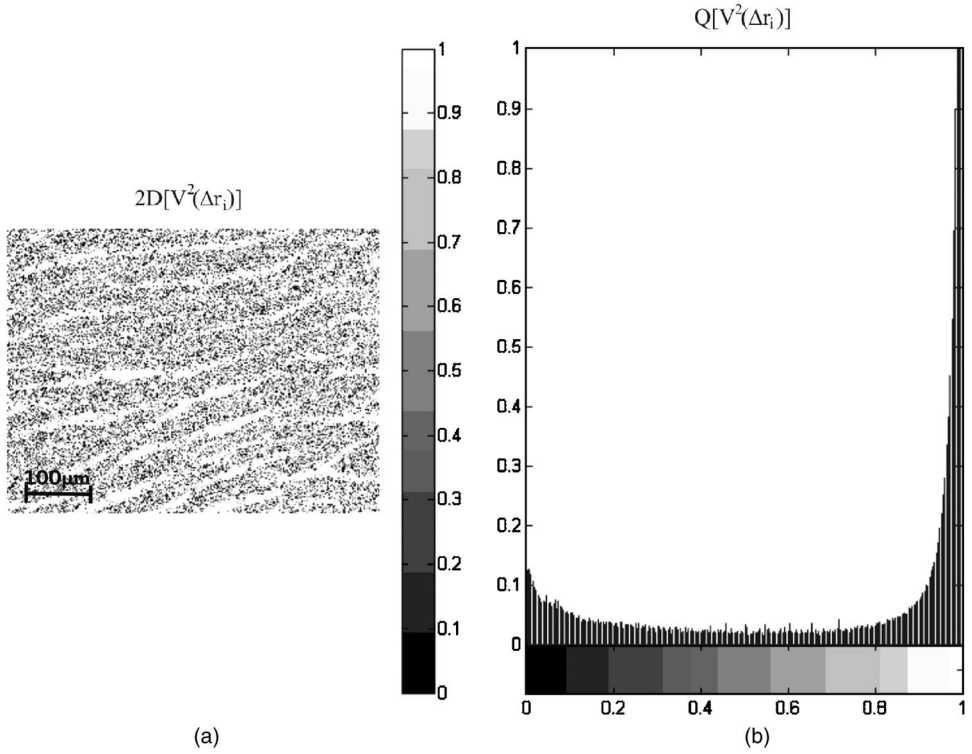

Fig. 6 (a) Coordinate and (b) statistical structure of CDMP of MT image.

$$E_x(r) = \{I_0[\sin^2 \alpha(r) + \cos^2 \alpha(r)\tan^2 \beta(r)]\}^{1/2},$$

$$E_y(r) = \{I_0[\cos^2 \alpha(r) + \sin^2 \alpha(r)\tan^2 \beta(r)]\}^{1/2}. \quad (32)$$

It follows from Eqs. (31) and (32) that the CDMP of BT image [Eqs. (23) and (27)] appears to be a parameter that is sensitive to orientation-phase architectonic changes.

"Optically thin" ($\tau \leqslant 0.1$) frozen histological sections of the BT of the following types were used as the objects of investigation:

1. Physiologically normal [Fig. 9(a)] and dystrophically changed [Fig. 9(b)] myocardium muscle tissue (MT),

2. Physiologically normal [Fig. 9(c)] tissue of cannon bone and bone tissue (BnT) affected with osteoporosis [Fig. 9(d)].

The technique of freezing of BT thin layers to "nitrogen" temperatures provided practically complete identity with them morphologically *in vivo* and *in vitro*. Histological sections of physiologically changed MT and BnT were taken in areas that do not correspond to localization of pathological changes in architectonics (psoriasis, muscular dystrophy). From the medical point of view such samples are "conventionally" normal. Traditional histochemical investigations do not show any differences in their physiological state.

Morphological structure of such BTs architectonics is different. MT is formed by quasiordered myosin fibrils and fibers forming bundles [Fig. 9(b)] with the birefringence index of their substance $\Delta n \approx 1.5 \times 10^{-3}$. The BnT architectonics is formed by oriented collagen fibers, which are mineralized by the hydroxylapathite crystals[21] ($\Delta n \approx 1.1 \times 10^{-1}$) [Fig. 9(d)].

Early (preclinical) degenerative-dystrophic changes of such tissues are formed morphologically according to various "scenarios."[22] Myosin fibrils and fibers under the unchanged birefringence level disorder within mono-oriented MT bundles. The osteoporosis-affected MT presents a decrease of hydroxylapathite crystals concentration ($\Delta n \approx 10^{-2}$ to 10^{-3}) under an unchanged orientation structure of the collagen net.

Coordinate distributions of the complex degree of mutual polarization of images of physiologically normal and degeneratively and/or dystrophically changed MT and BnT are illustrated in Figs. 10(a), 11(a), 10(b), and 11(b), correspondingly.

Measuring the intensity values, azimuths, and ellipticities of polarization necessary for calculation of $2D[V^2(\Delta r_i)]$ of images of all types of BT was performed for discretization parameter $\Delta r_i = 1$ pixel.

Figures 10(c), 10(d), 11(c), and 11(d) present histograms of probability distributions of CDMP $\{2D[V^2(\Delta r_i)]\}$ values.

Distributions $2D[V^2(\Delta r_i)]$ of images of physiologically normal BT of both types are rather close in their structure—mainly formed by the areas [Figs. 10(a) and 11(a)] with maximally correlated state of polarization $V^2(\Delta r_i) \to 1$. Statistically the principal extreme of corresponding histograms $Q[V^2(\Delta r_i)]$ points to this [Figs. 10(c) and 11(c)]. Alongside this, $2D[V^2(\Delta r_i)]$ of such images contain a small number of areas of intermediate values of CDMP $[0 \leqslant V^2(\Delta r_i) \leqslant 1]$ with additional extreme $Q[V^2(\Delta r_i)]$ corresponding to them.

Coordinate distributions CDMP of the degeneratively and/or dystrophically changed BT samples images is formed by the areas for which the value of CDMP changes within wide limits $[0 \leqslant V^2(\Delta r_i) \leqslant 1]$ [Figs. 10(b) and 11(b)]. Corresponding histograms $Q[V^2(\Delta r_i)]$ contain the totality of equiprobable extrema, enough for the whole range of changing the

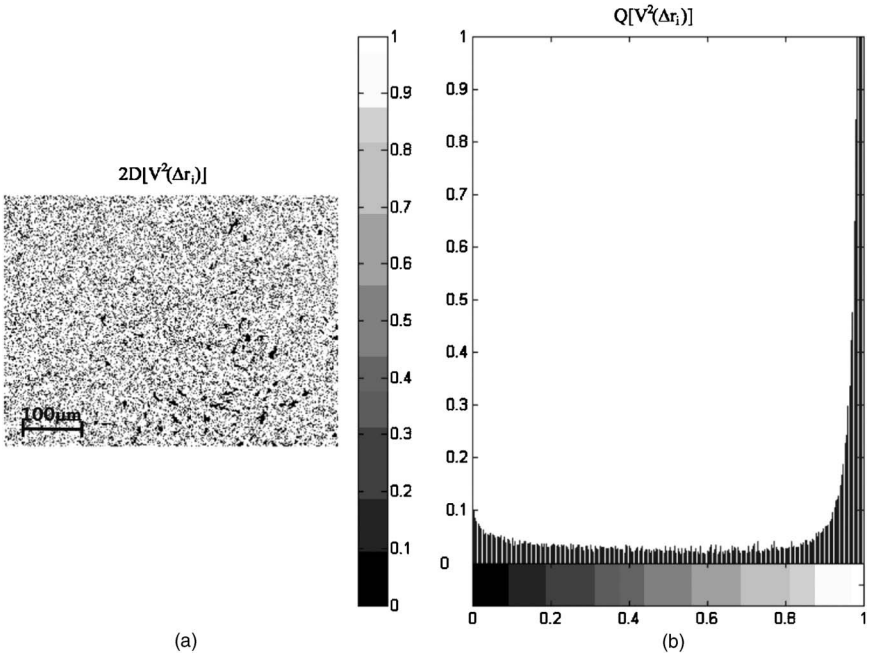

Fig. 7 Polarization-correlation structure of kidney tissue speckle-image.

CDMP value of images of both MTs [Fig. 10(d)] and BTs [Fig. 11(d)].

The dependences $Q[V^2(\Delta r_i)]$ objectively characterize the totality of statistic moments of values of CDMP of the first to fourth orders (see Table 4).

The investigated structure of $2D[V^2(\Delta r_i)]$ of physiologically normal and degeneratively and/or dystrophically changed BT images is closely connected with various morphological structure of their architectonics.

The packing and well-ordering of myosin and collagen fibrils of physiologically normal MTs and BnTs within rather

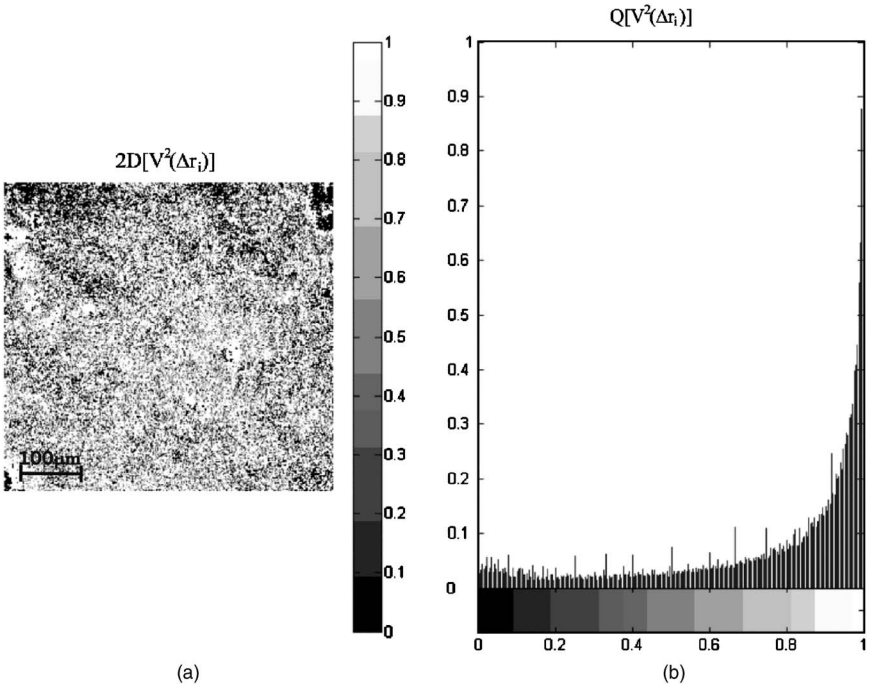

Fig. 8 Coordinate (a) and statistical (b) structure of CDMP of spleen tissue image.

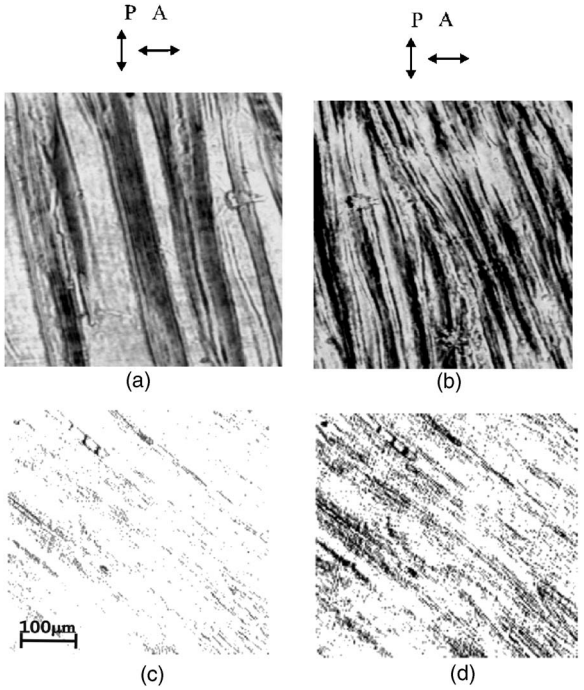

Fig. 9 Images of architectonics of physiologically (a) normal MT, (c) BnT, and dystrophical changed (b) MT and (d) BnT (with osteoporosis) in crossed polarizer (P) and analyzer (A). The arrows depict the orientation of the optical axes of both polarizer (A) and analyzer (B), respectively.

large geometric domains of their architectonic nets according to Eqs. (18), (19), and (23) causes high correlation similarity $[V^2(\Delta r_i) \rightarrow 1]$ of polarization states of corresponding points in their images. However, within the domain itself, the degree of mutual polarization of BT images points extremely increases again.

The inverse tendency is observed for 2-D distributions of CDMP images of physiologically changed samples of both types of BTs.

Morphological degenerative-dystrophic changes of MT are accompanied by fibril packing disorder in MT myosin bundles. From an optical point of view, such a process is similar to an increase of the angle interval between polarization azimuth of illuminating laser beam α_0 and the highest speed axis $\rho(r)$ direction of optically anisotropic structures. According to Eqs. (22) and (23) various states of polarization $\alpha(r)$ and $\beta(r)$ of laser oscillations will be formed in corresponding points of MT image. Thus, the fluctuations of CDMP value increase while corresponding statistic distributions $Q[V^2(\Delta r_i)]$ will be transformed into the totality of rather equiprobable extrema [Fig. 10(d)].

Optically, early manifestation of BnT osteoporosis can be represented by coordinate modulation of phase shifts $\delta(r)$, shown by hydroxylapathite crystals between orthogonal polarization components E_{0x} and E_{0y} of the illuminating laser radiation, forming a corresponding coherent image. Such modulation at the unchanged orientational structure $\rho(r)$ of collagen fibers is the main reason of forming polarizationally inhomogeneous $\alpha(r)$ and $\beta(r)$ parts of the BnT image, and value of $V^2(\Delta r_i)$ connected with this becomes statistical.

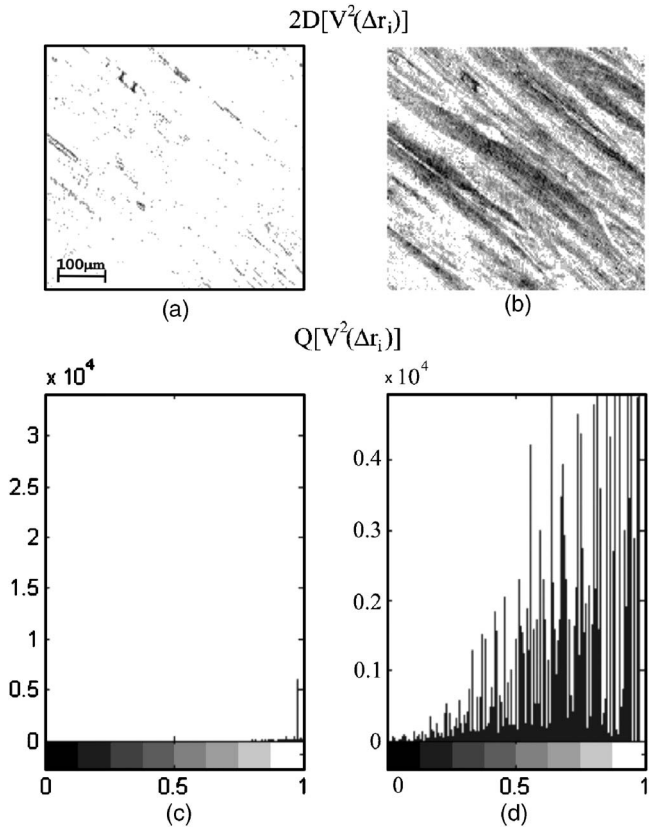

Fig. 10 (a) and (b) coordinate and (c) and (d) statistical structure of CDMP of images of healthy (a) and (c) and pathological changed (osteoporosis) (b) and (d) BnT.

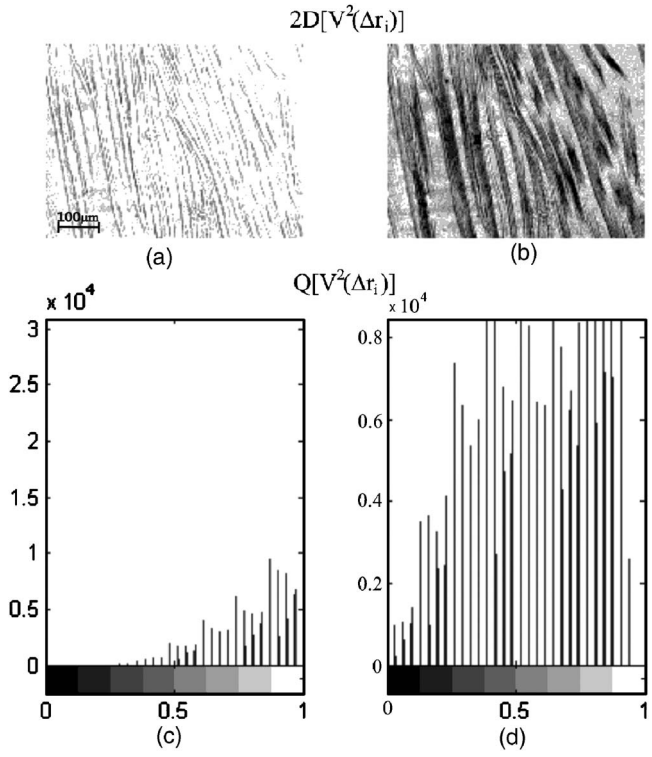

Fig. 11 (a) and (b) coordinate and (c) and (d) statistical structure of CDMP of images of healthy (a) and (c) and pathological changed (dystrophically changed) (b) and (d) MT.

Table 4 Statistics of the first to fourth orders of CDMP of BT images.

MT (37 samples)			BnT (34 samples)		
	Normal	Dystrophically Changed		Normal	Affected by Osteoporosis
M_{V2}	0.18±4%	0.96±11%	M_{V2}	0.24±6%	0.85±13%
σ_{V2}	0.11±6%	0.67±17%	σ_{V2}	0.18±8%	0.45±16%
A_{V2}	67.4±11%	589.7±19%	A_{V2}	87.3±13%	967.7±23%
E_{V2}	32.2±15%	451.3±23%	E_{V2}	74.9±17%	798.3±25%

A comparative analysis of statistic moments of first to fourth orders of the $V^2(\Delta r_i)$ value of coherent images of the groups (see Table 3) of physiologically normal $(M^*_{V2}, \sigma^*_{V2}, A^*_{V2}, E^*_{V2})$ and pathologically changed $(M_{V2}, \sigma_{V2}, A_{V2}, E_{V2})$ BT of both types demonstrates the following:

$$M_{V2} \geq M^*_{V2}, \quad \sigma_{V2} \geq \sigma^*_{V2}, \quad A_{V2} \geq A^*_{V2}, \quad E_{V2} \geq E^*_{V2}. \tag{33}$$

We can see that if the probability distributions of the following form

$$Q[V^2(\Delta r_i)] = \begin{cases} 1[V^2(\Delta r_i) = 1] \\ \to 0[V^2(\Delta r_1) \neq 1], \end{cases}$$

[Figs. 10(c) and 11(c)] transform into a random $(0 \leq Q[V^2(\Delta r_i)] \leq 1)$. In this case, the corresponding statistical moments of CDMP values of degeneratively and/or dystrophycally BT images become larger. Such differences are the most pronounced (by one order of the value) for the third and fours statistical moments of CDMP.

7 Conclusions

On the basis of polarizational measurements technique of 2-D distributions of CDMP of BT images the interconnection between the statistical moments of CDMP values and the optical-geometrical structure of degeneratively and/or dystrophycally changed the MT and BnT architectonics nets. The obtained information concerning the polarization-correlation structure of images correspond to different BT morphological structures can be used for elaboration of new methods for their analysis of physiological state.

References

1. M. S. Patterson, S. Andersson-Engels, B. C. Wilson, and E. K. Osei, "Absorption-spectroscopy in tissue-simulating materials—a theoretical and experimental-study of photon paths," *Appl. Opt.* **34**, 22–30 (1995).
2. R. R. Alfano and J. G. Fujimoto, eds., *Advances in Optical Imaging and Photon Migration*, Vol. **2** of *Topics in Optics and Photonics Series*, Optical Society of America, Washington, DC (1996).
3. S. Bartel and A. H. Hielscher, "Monte Carlo simulation of the diffuse backscattering Mueller matrix for highly scattering media," *Appl. Opt.* **39**, 1580–1588 (2000).
4. S. P. Morgan, M. P. Khong, and M. G. Somekh, "Effects of polarization state and scatterer concentration on optical imaging through scattering media," *Appl. Opt.* **36**, 1560–1565 (1997).
5. S. G. Demos and R. R. Alfano, "Optical polarization imaging," *Appl. Opt.* **36**, 150–155 (1997).
6. S. L. Jacques, J. R. Roman, and K. Lee, "Imaging superficial tissues with polarized light," *Lasers Surg. Med.* **26**, 119–129 (2000).
7. M. Born and E. Wolf, *Principles of Optics*, Cambridge Univ. Press, Cambridge (1999).
8. A. G. Ushenko and V. P. Pishak, "Laser polarimetry of biological tissue: principles and applications," in *Coherent-Domain Optical Methods: Biomedical Diagnostics, Environmental and Material Science*, V. Tuchin, Ed., pp. 67–93, Kluwer Academic, Boston (2004).
9. V. Sankaran, K. Schonenberger, J. T. Walsh, Jr., and D. J. Maitland, "Polarization discrimination of coherently propagation light in turbid media," *Appl. Opt.* **38**, 4252–4261 (1999).
10. G. Jarry, E. Steimer, V. Damaschini, M. Epifanie, M. Jurczak, and R. Kaiser, "Coherence and polarization of light propagating through scattering media and biological tissues," *Appl. Opt.* **37**, 7357–7367 (1998).
11. E. I. Olar, A. G. Ushenko, and Y. A. Ushenko, "Correlation microstructure of the Jones matrices for multifractal networks of biotissues," *Laser Phys.* **7**, 1012–1019 (2004).
12. E. I. Olar, A. G. Ushenko, and Yu. A. Ushenko, "Polarization correlation measurements of the phase tomograms of optically anisotropic biofractals," *Laser Phys.* **8**, 1015–1022 (2004).
13. F. Gori, "Matrix treatment for partially polarized, partially coherent beams," *Opt. Lett.* **23**, 241–243 (1998).
14. J. Ellis and A. Dogariu, "Complex degree of mutual polarization," *Opt. Lett.* **29**, 536–538 (2004).
15. E. Wolf, "Significance and measurability of the phase of a spatially coherent optical field," *Opt. Lett.* **28**, 5–6 (2003).
16. M. Mujat and A. Dogariu, "Polarimetric and spectral changes in random electromagnetic fields," *Opt. Lett.* **28**, 2153–2155 (2003).
17. J. Ellis, A. Dogariu, S. Ponomarenko, and E. Wolf, "Interferometric measurement of the degree of polarization and control of the contrast of intensity fluctuations," *Opt. Lett.* **29**, 1536–1538 (2004).
18. M. Mujat, A. Dogariu, and G. S. Agarwal, "Correlation matrix of a completely polarized, statistically stationary electromagnetic field," *Opt. Lett.* **29**, 1539–1541 (2004).
19. S. Jiao and L. V. Wang, "Two-dimensional depth-resolved Mueller matrix of biological tissue measured with double-beam polarization-sensitive optical coherence tomography," *Opt. Lett.* **27**, 101–103 (2002).
20. O. V. Angelsky, G. V. Demyanovsky, A. G. Ushenko, D. N. Burcovets, and Y. A. Ushenko, "Wavelet analysis of two-dimensional birefringence images of architectonics in biotissues for diagnosing pathological changes," *J. Biomed. Opt.* **9**(4), 679–690 (2004).
21. O. V. Angel'skii, O. G. Ushenko, D. N. Burkovets, O. D. Arkhelyuk, and Y. A. Ushenko, "Polarization-correlation studies of multifractal structures in biotissues and diagnostics of their pathologic changes," *Laser Phys.* **10**(5), 1136–1142 (2000).
22. A. G. Ushenko, "The vector structure of laser biospeckle fields and polarization diagnostic of collagen skin structures," *Laser Phys.* **10**(5), 1143–1150 (2000).